

Supplementary Information

Alkane-Length Sorting Using Activated Pillar[5]arene Crystals

Tomoki Ogoshi^{a,b,}, Ryuta Sueto,^a Yukie Hamada,^a Kazuki Doitomi,^c Hajime Hirao,^{b,c,d}*

Yoko Sakata,^a Shigehisa Akine,^a Takahiro Kakuta^a and Tada-aki Yamagishi^a

^aGraduate School of Natural Science and Technology, Kanazawa University, Kakumamachi, Kanazawa, 920-1192, Japan

^bJST, PRESTO, 4-1-8 Honcho, Kawaguchi, Saitama, 332-0012, Japan

^cDepartment of Biology and Chemistry, City University of Hong Kong, Tat Chee Avenue, Kowloon, Hong Kong, China

^dDivision of Chemistry and Biological Chemistry, School of Physical and Mathematical Sciences, Nanyang Technological University, 21 Nanyang Link, 637371, Singapore

Table of Contents

1. Materials	S2
2. Methods	S2
3. Sample Preparations	S3
4. Computational Details	S17
5. References	S18

1. Materials

All solvents and reagents were used as supplied. Pillar[5]arene bearing 10 ethyl groups (**1**) was synthesized according to the previous paper.^{S1}

2. Methods

2.1 Solution NMR

Solution ¹H NMR spectra were recorded at 500 with a JEOL-ECA500 spectrometer.

2.2 Gas Chromatography

Gas chromatography (GC) analyses were performed on a Shimadzu GC-2014 gas chromatograph with a capillary column (Shimadzu capillary column Rtx-1: 12457) using acetone as an internal standard. The following GC method was used; the oven was programmed from 40 °C, ramped at 10 °C min⁻¹ increments to 250 °C 4 min hold, the total run time was 25 min; injection temperature 250 °C; detection temperature 250 °C with hydrogen, air, and make-up flow-rates of 35, 350, and 35 mL min⁻¹, respectively; helium (carrier gas) flow-rate 1.76 mL min⁻¹.

2.3 Powder X-Ray Diffraction

Laboratory powder X-ray diffraction (PXRD) measurements were performed on a Rigaku Smart Lab high-resolution diffractometer.

2.4 Computational Method

Molecular mechanics (MM) calculations were executed to calculate binding energies between several *n*-alkanes (**C6-C16**) and pillar[5]arene(s). For this purpose, the Forcite program available in Materials Studio 8.0 was used,^{S2} and molecules were described by use of the COMPASS II force field.^{S3,4} We evaluated binding energies for the three types of models: 1:1 complexes (model 1), herringbone structures (model 2), and one-dimensional channel structures (model 3). Models 1 and 3 were built from the X-ray structure of **1** ⊃ **C8** complexes, while model 2 was prepared from the X-ray structure of **1** ⊃ **C6** complexes. Binding energies were calculated using the following equation:

$$E_{(\text{bind})} = E_{(\text{model_with_}n\text{-alkane})} - \{E_{(\text{model_without_}n\text{-alkane})} + E_{(n\text{-alkane})}\}$$

where the E values are energies of geometry-optimized molecules.

3. Sample Preparation

3.1 Activation of Crystals of Pillar[5]arene 1

Pillar[5]arene **1** was dissolved in acetone, and then the evaporation of acetone afforded crystals **1**. Drying crystals **1** at 80 °C under reduced pressure for 24 h was sufficient to de-solvate all the acetone molecules and afforded activated crystals of **1**. Removing acetone was confirmed by ^1H NMR measurement (**Fig. S1a**). No proton signals from acetone indicate complete activation of crystals **1**.

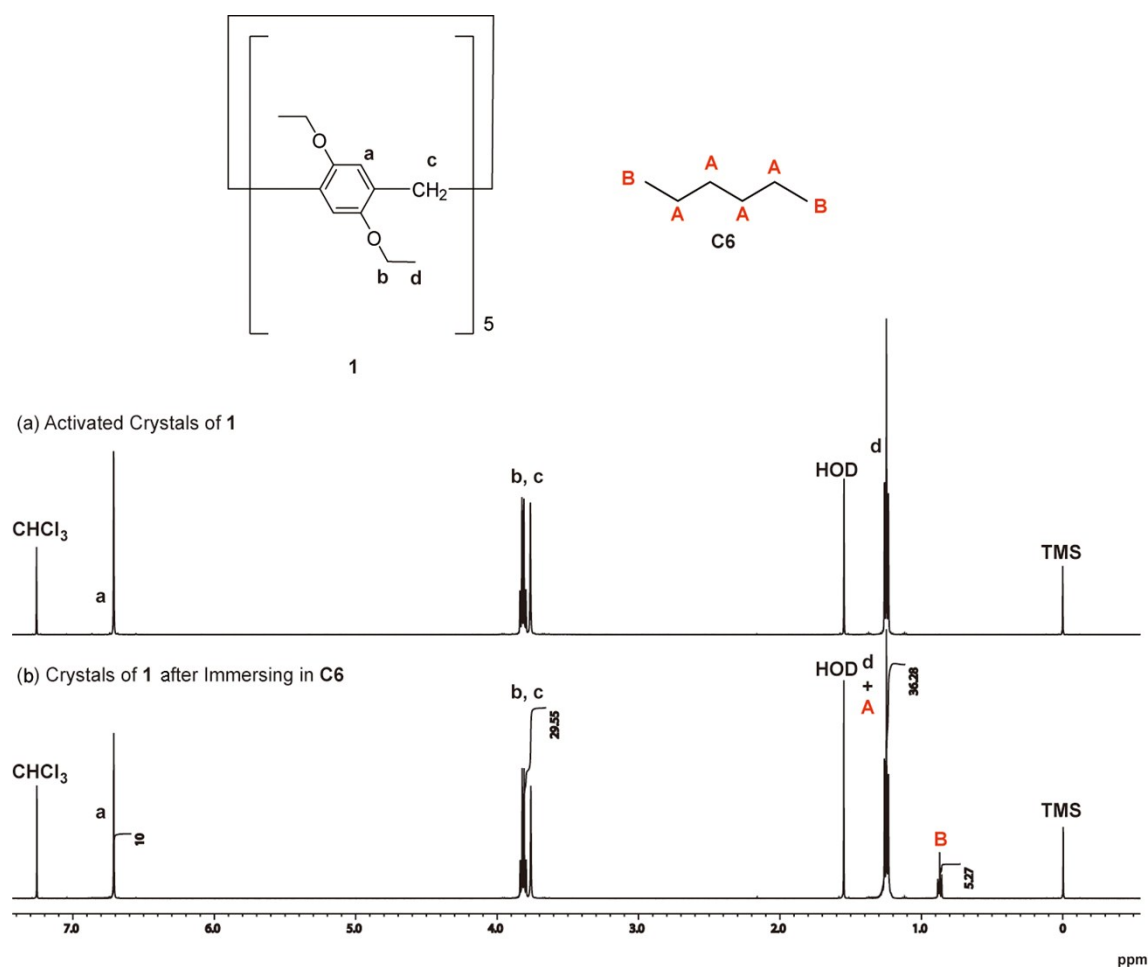


Fig. S1 ^1H NMR spectra (25 °C, CDCl_3) of (a) activated pillar[5]arene **1** and (b) crystals of **1** after immersing in **C6** for 12 h. The ratio of *n*-alkane uptake was determined from integration ratio between peaks a (proton signal of **1**) and B (proton signal of **C6**).

3.2 *n*-Alkane Uptake Experiments by Immersing Activated Crystals of **1** in *n*-

Alkane

Activated crystals of **1** (20 mg) was immersed in a sealed 5 mL vial containing 1 mL of bulk *n*-alkane at 25 °C. To remove un-complexed *n*-alkane, the crystals were washed with cyclohexane because pillar[5]arenes do not form complexes with cyclohexane. Uptake of *n*-alkane guest by **1** was monitored by completely dissolving the crystals in CDCl₃ and measuring the ratio of *n*-alkane to pillar[5]arene **1** by ¹H NMR (**Fig. S1b**). We attempted to monitor the time-dependent uptake of **C6** by activated crystals of **1** using ¹H NMR (**Fig. S4**), but this trial failed because it took only a few seconds to complete the uptake process. Longer *n*-alkanes were also taken up on immersing activated crystals of **1** in the bulk liquid *n*-alkanes. When **C12** and **C16** were used as bulk liquid *n*-alkanes, it took ca. 120 s and 180 s to complete the uptake process, respectively.

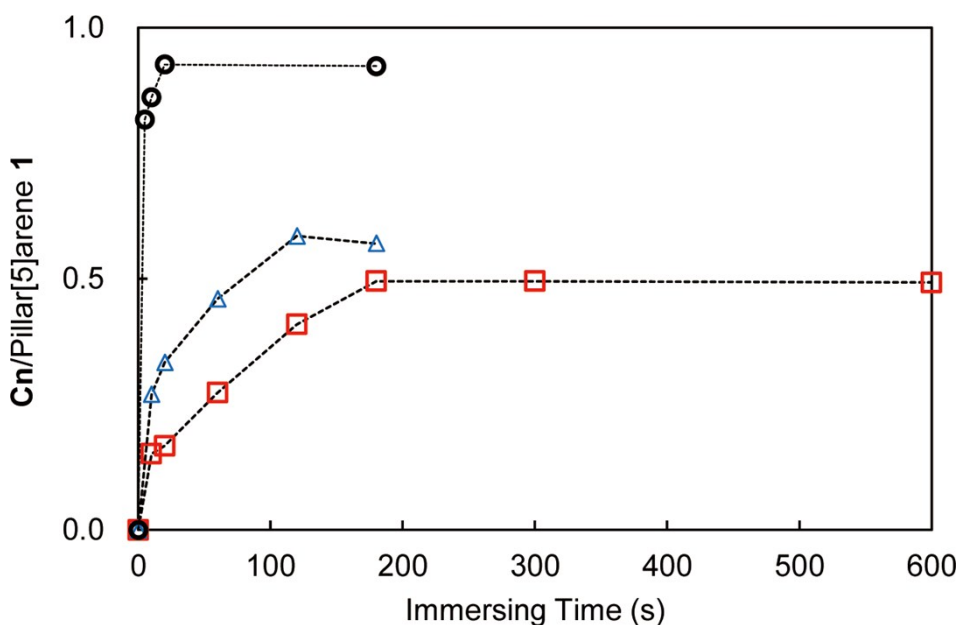


Fig. S4 Time-dependent uptake of **C6** (black circles), **C12** (blue triangles) and **C16** (red squares) by activated crystals of **1**.

3.3 Re-activated of Pillar[5]arene Crystals of **1** for Reuse

Host-guest complex crystals **1** containing **C6** at 80 °C under reduced pressure for 12 h afforded re-activated crystals **1**. Complete removal of **C6** was checked by ^1H NMR. The activated crystals of **1** took up **C6** again by immersing the crystals into **C6**, which was determined by ^1H NMR and TGA (**Fig. S2**).

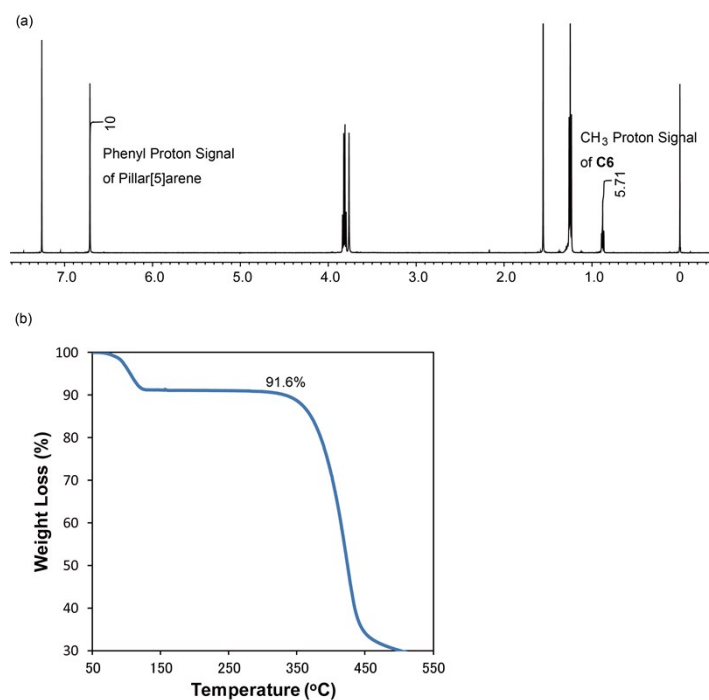


Fig. S2 (a) ^1H NMR spectrum (25 °C, CDCl_3) and (b) TGA trace of the re-activated crystals **1** after immersing in **C6** for 12 h. The appearance of **C6** signal from ^1H NMR (**Fig. S2a**) and the weight loss until 150 °C from TGA (**Fig. S2b**) indicate re-uptake of **C6** by the re-activated crystals of **1**.

3.4 *n*-Alkane Shape Sorting Experiments by Immersing Activated Crystals of **1** in C_6H_{14} Isomers

Activated crystals of **1** (20 mg) was immersed in a sealed 5 mL vial containing equal volume of bulk C_6H_{14} isomers [*n*-hexane (**C6**), 2-methylpentane, 3-methylpentane, 2,3-dimethylbutane and 2,2-dimethylbutane] at 25 °C. To remove un-complexed alkanes, the crystals were washed with cyclohexane. Composition of alkane guests up-taken by activated crystals of **1** was monitored by completely dissolving the crystals in acetone and measuring by gas chromatography (**Fig. S3**). The activated crystals of **1** only formed complexes with linear alkane (**C6**).

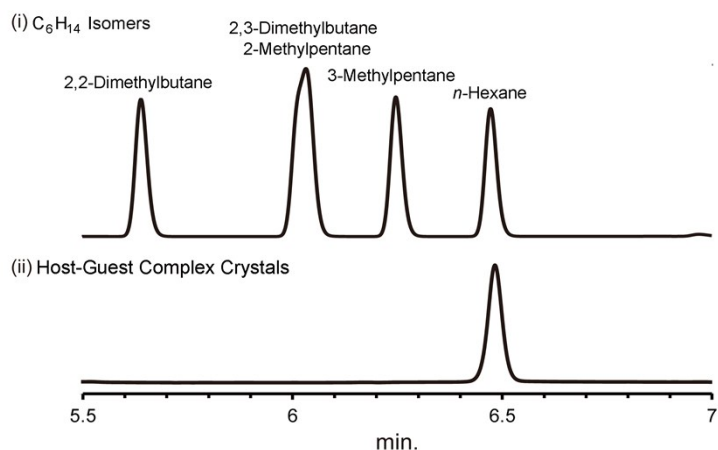


Fig. S3 Gas chromatograms of (i) an equimolar mixture of C₆H₁₄ isomers and (ii) host-guest complex crystals prepared by immersing activated crystals of **1** into equimolar mixtures of C₆H₁₄ isomers for 12 h. The gas chromatogram of the mixture showed four peaks from the five C₆H₁₄ isomers with two peaks for two of the isomers overlapping with each other at the same position (**Fig. S4(i)**). However, only a single peak corresponding to **C6** was observed in the gas chromatogram of the host-guest complex crystals after immersion in the mixture of the C₆H₁₄ isomers (**Fig. S4(ii)**), which indicates that activated crystals of **1** were able to sort linear **C6** from the mixture of C₆H₁₄ isomers.

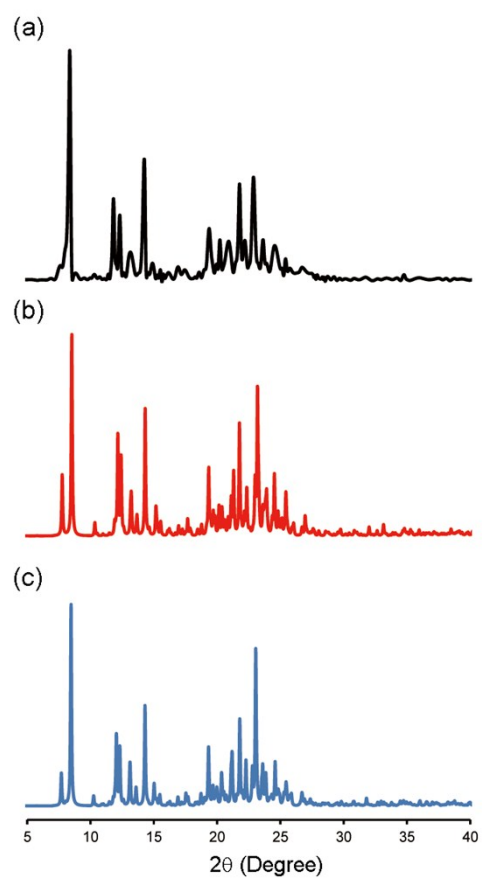


Fig. S5 PXRD patterns of (a) host-guest complex crystals of **1** with **C7** (black line), simulation from X-ray crystal structures of (b) **1**⊃**C6** (red line) and (c) **1**⊃**C7** complexes (blue line).

3.3 Determination of Stoichiometry of Host-Guest Complex Crystals

Activated crystals of **1** (20 mg) was immersed in a sealed 5 mL vial containing 1 mL of mixtures of bulk *n*-alkanes at 25 °C for 12 h. The immersing time (12 h) is enough to reach the equilibrium state by monitoring uptake of *n*-alkane (**Fig. 2S**). To remove uncomplexed *n*-alkanes, the crystals were washed with cyclohexane. Stoichiometry of the complex crystals after the immersion was monitored by completely dissolving the crystals in CDCl₃ and measuring the ratio of *n*-alkane to pillar[5]arene **1** by ¹H NMR (**Figs. S6-S16**).

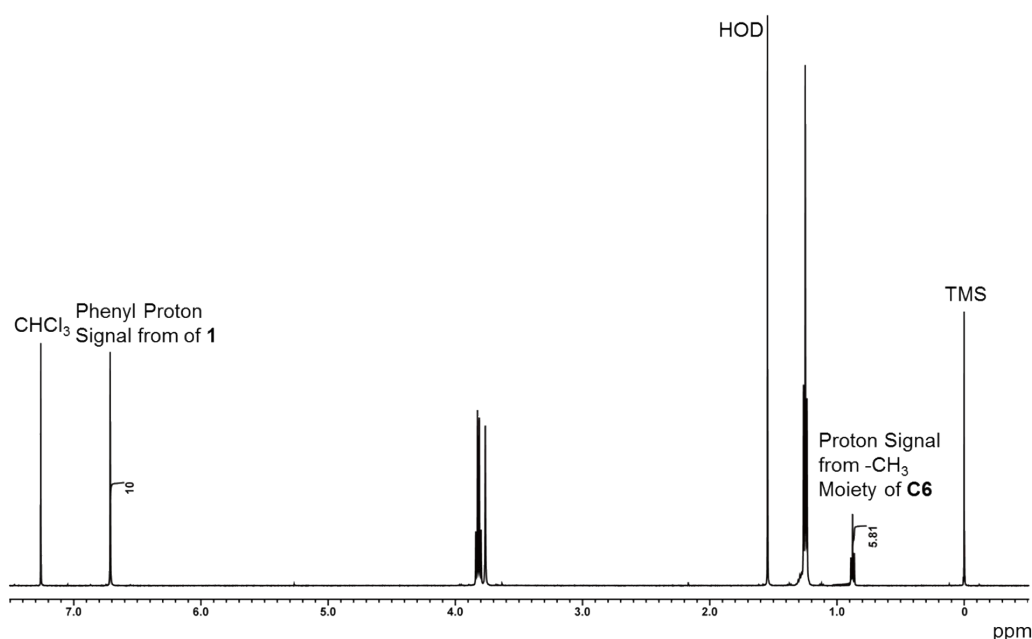


Fig. S6 ¹H NMR spectrum (25 °C, CDCl₃) crystals of **1** after immersing in **C6** for 12 h. The stoichiometry was determined from integration ratio between proton signals from methyl moiety of **C6** and phenyl moiety of **1**.

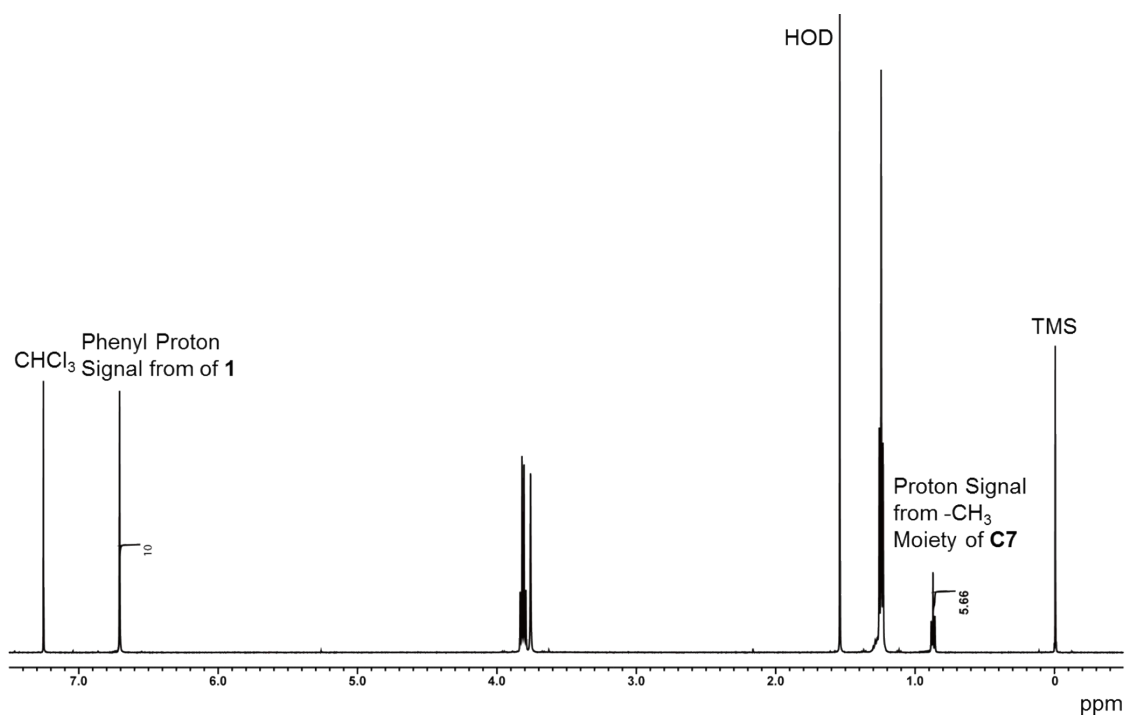


Fig. S7 ^1H NMR spectrum (25 $^\circ\text{C}$, CDCl_3) crystals of **1** after immersing in **C7** for 12 h. The stoichiometry was determined from integration ratio between proton signals from methyl moiety of **C7** and phenyl moiety of **1**.

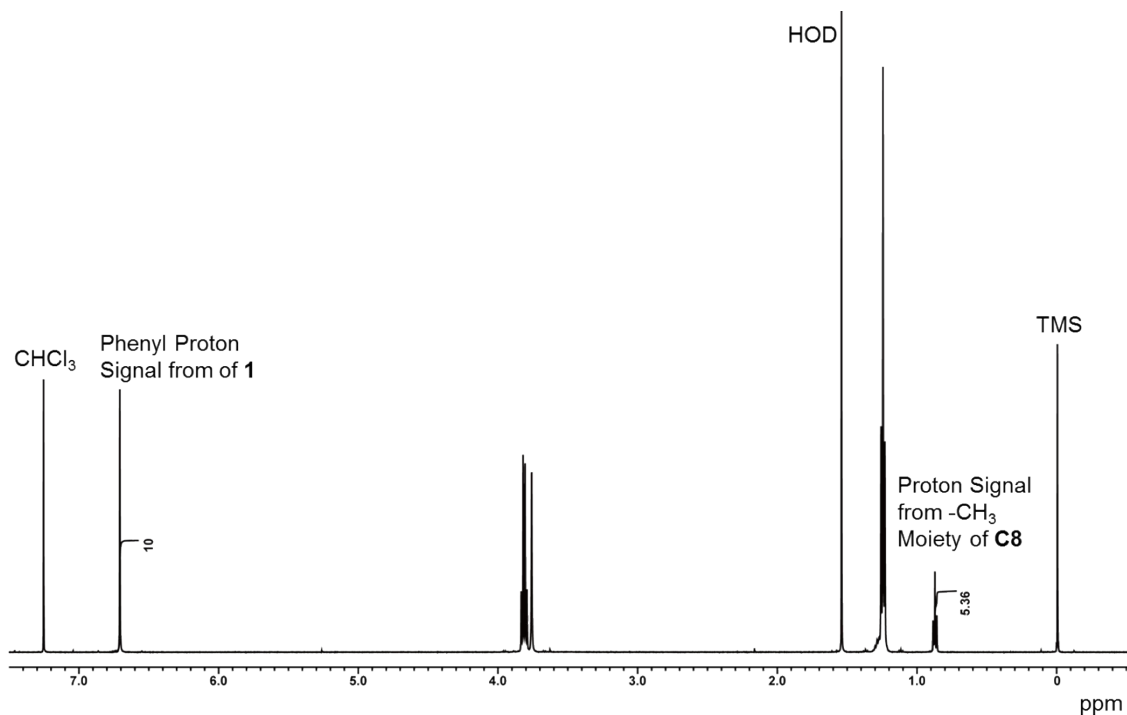


Fig. S8 ^1H NMR spectrum (25 $^\circ\text{C}$, CDCl_3) crystals of **1** after immersing in **C8** for 12 h. The stoichiometry was determined from integration ratio between proton signals from methyl moiety of **C8** and phenyl moiety of **1**.

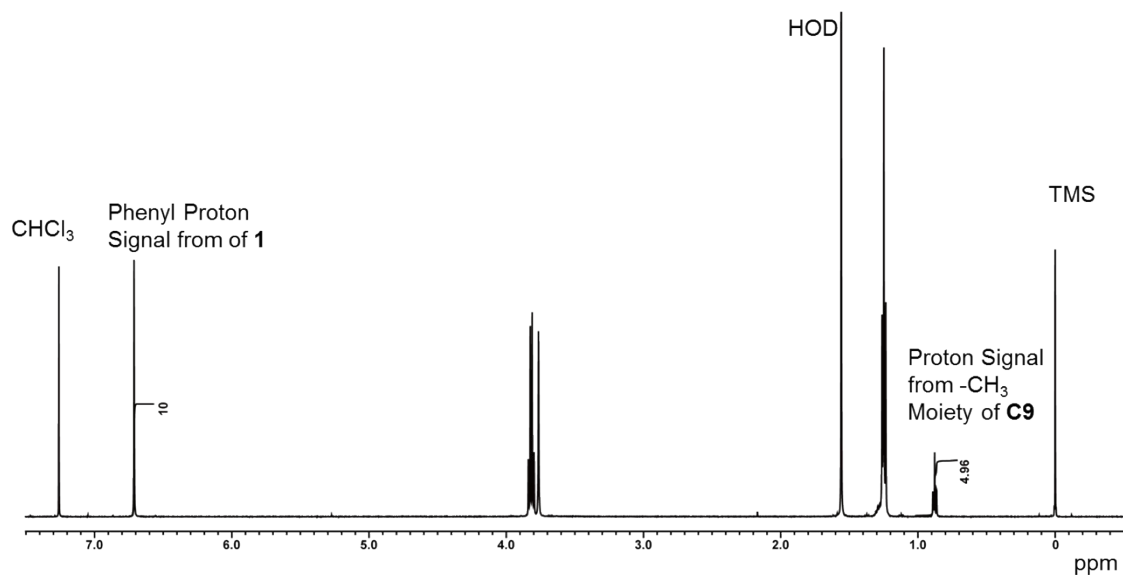


Fig. S9 ¹H NMR spectrum (25 °C, CDCl₃) crystals of **1** after immersing in **C9** for 12 h. The stoichiometry was determined from integration ratio between proton signals from methyl moiety of **C9** and phenyl moiety of **1**.

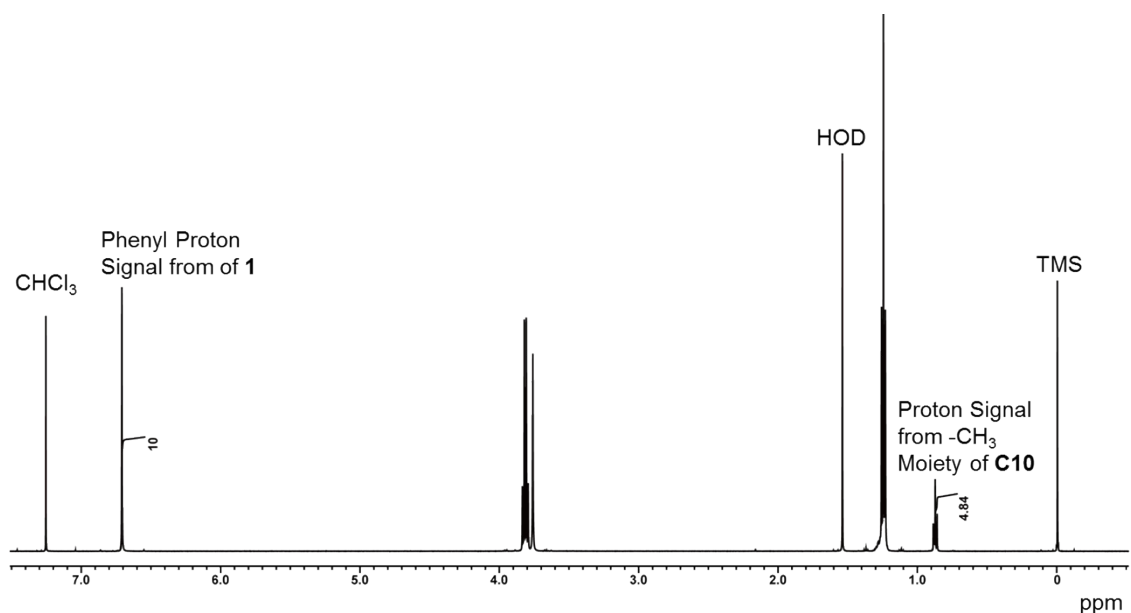


Fig. S10 ¹H NMR spectrum (25 °C, CDCl₃) crystals of **1** after immersing in **C10** for 12 h. The stoichiometry was determined from integration ratio between proton signals from methyl moiety of **C10** and phenyl moiety of **1**.

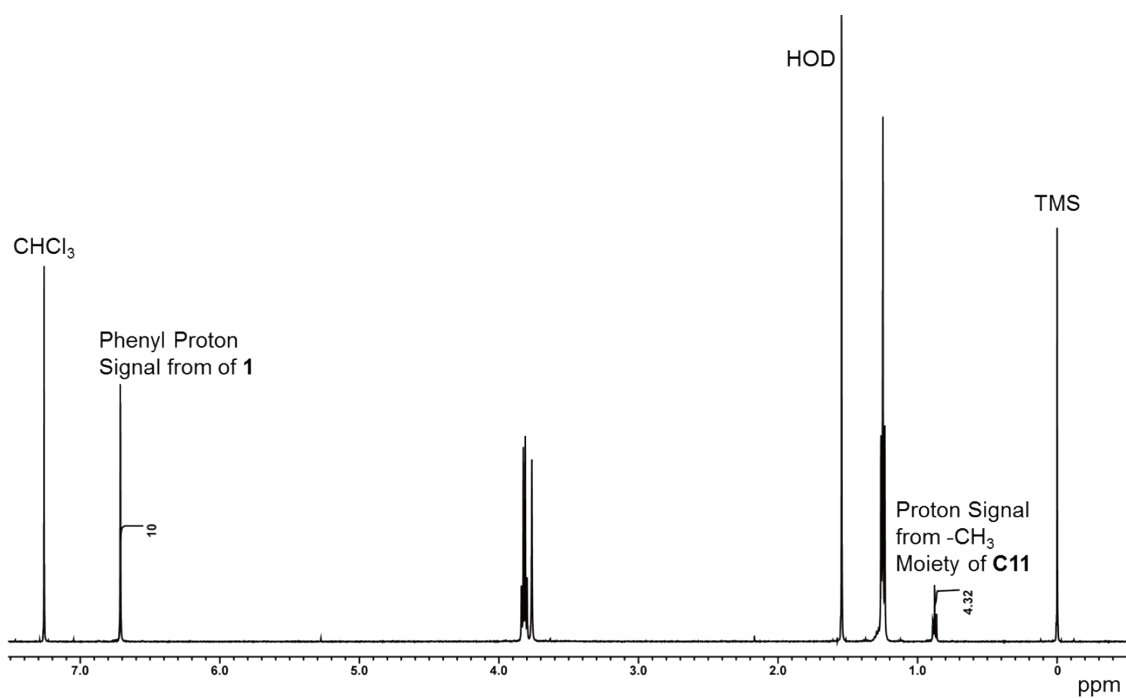


Fig. S11 ^1H NMR spectrum (25 $^\circ\text{C}$, CDCl_3) crystals of **1** after immersing in **C11** for 12 h. The stoichiometry was determined from integration ratio between proton signals from methyl moiety of **C11** and phenyl moiety of **1**.

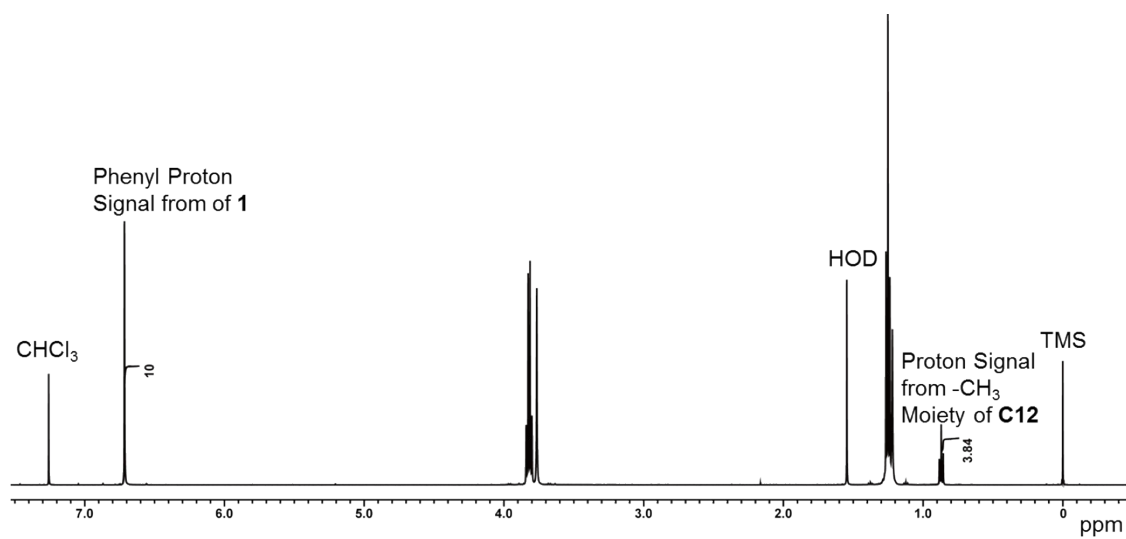


Fig. S12 ^1H NMR spectrum (25 $^\circ\text{C}$, CDCl_3) crystals of **1** after immersing in **C12** for 12 h. The stoichiometry was determined from integration ratio between proton signals from methyl moiety of **C12** and phenyl moiety of **1**.

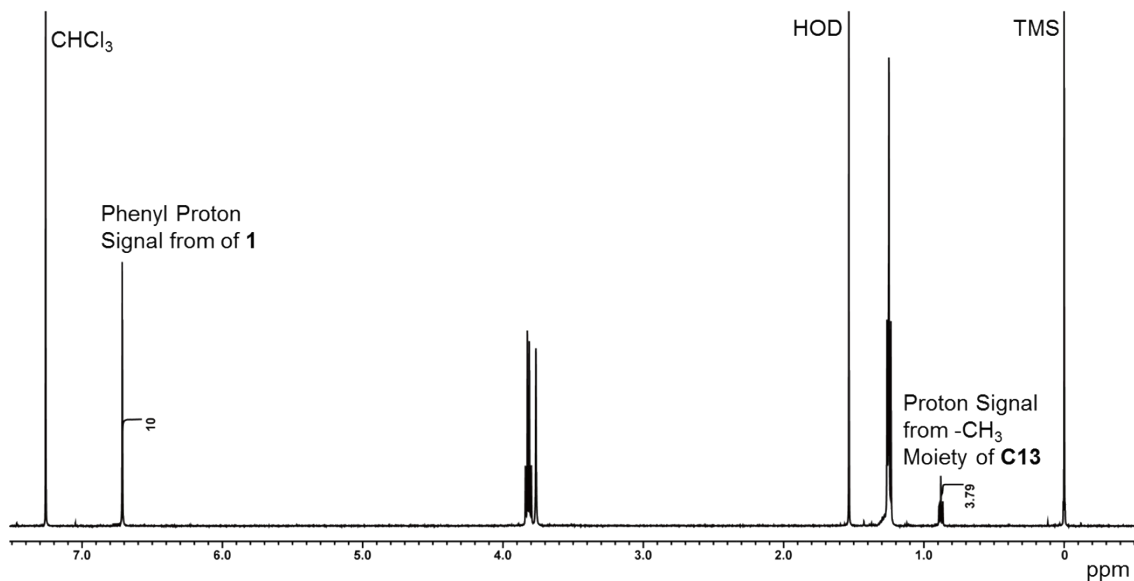


Fig. S13 ¹H NMR spectrum (25 °C, CDCl₃) crystals of **1** after immersing in **C13** for 12 h. The stoichiometry was determined from integration ratio between proton signals from methyl moiety of **C13** and phenyl moiety of **1**.

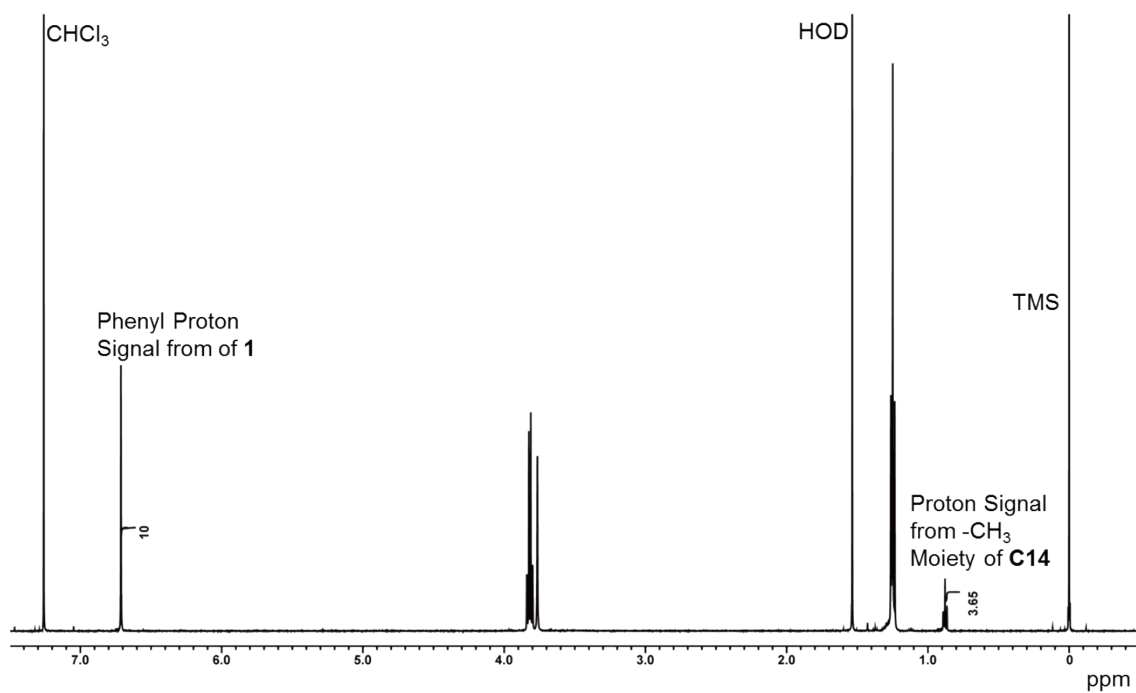


Fig. S14 ¹H NMR spectrum (25 °C, CDCl₃) crystals of **1** after immersing in **C14** for 12 h. The stoichiometry was determined from integration ratio between proton signals from methyl moiety of **C14** and phenyl moiety of **1**.

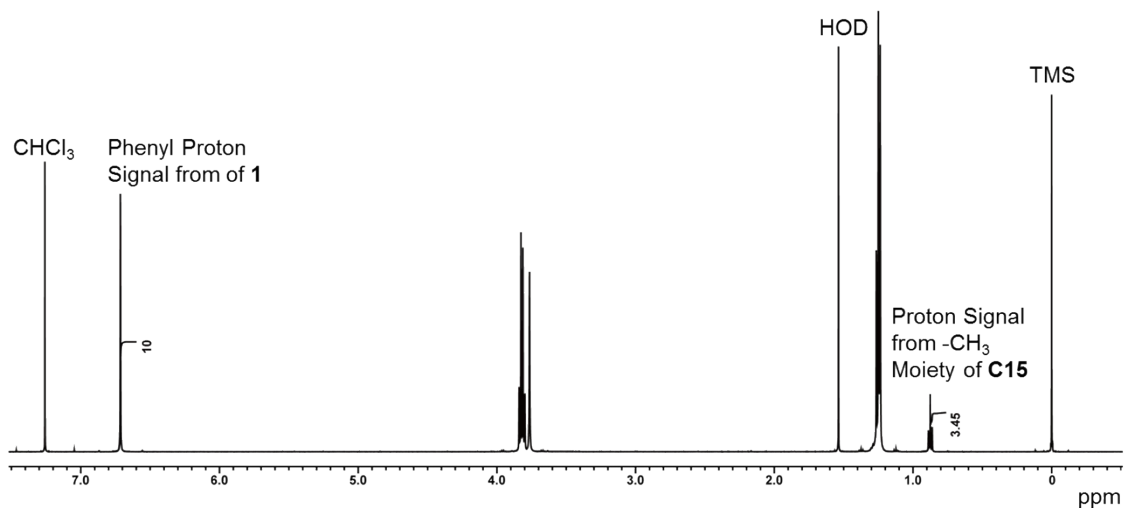


Fig. S15 ^1H NMR spectrum (25 $^\circ\text{C}$, CDCl_3) crystals of **1** after immersing in **C15** for 12 h. The stoichiometry was determined from integration ratio between proton signals from methyl moiety of **C15** and phenyl moiety of **1**.

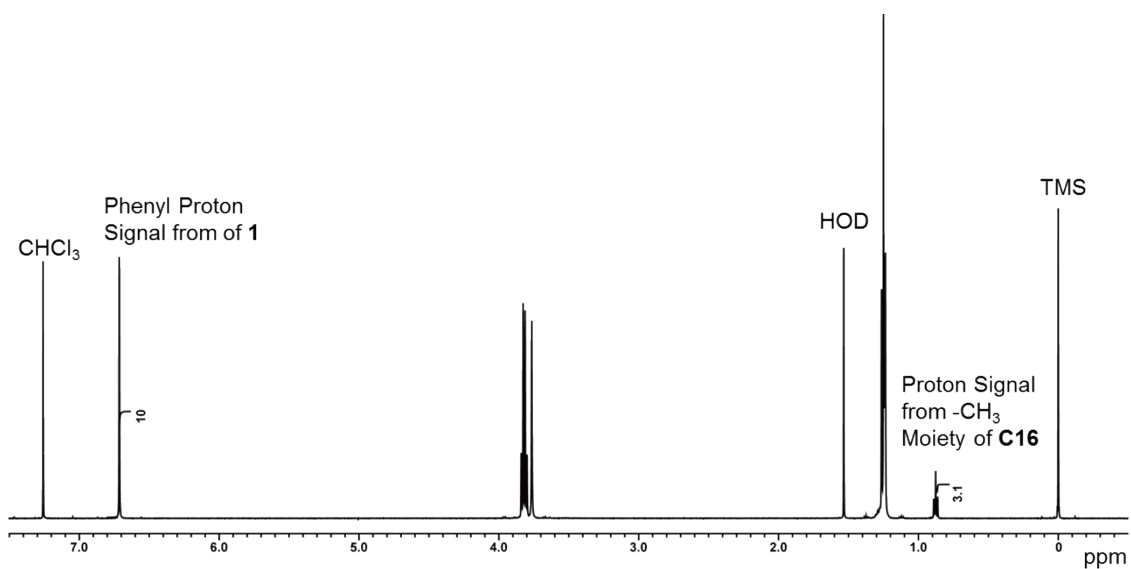
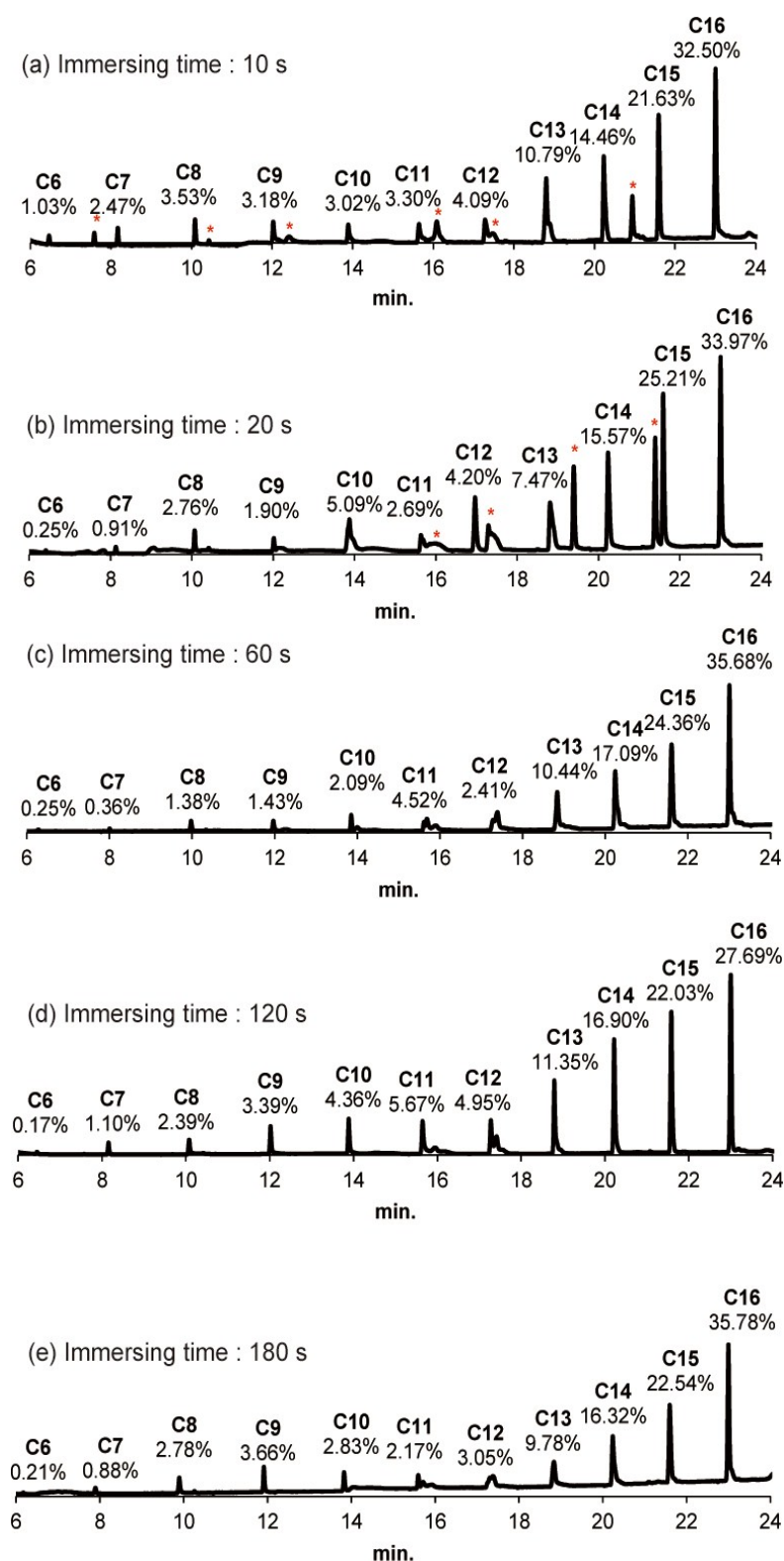


Fig. S16 ^1H NMR spectrum (25 $^\circ\text{C}$, CDCl_3) crystals of **1** after immersing in **C16** for 12 h. The stoichiometry was determined from integration ratio between proton signals from methyl moiety of **C16** and phenyl moiety of **1**.

3.4 *n*-Alkane Length Sorting by Immersing Activated Crystals of **1** in Mixture of Bulk *n*-Alkanes

Activated crystals of **1** (20 mg) was immersed in a sealed 5 mL vial containing bulk *n*-alkanes consisting of equal volume [total 5.5 mL = 0.5 mL \times 11 (C6-C16)] at 25 °C. To remove un-complexed *n*-alkanes, the crystals were washed with cyclohexane. Composition of *n*-alkane guests up-taken by activated crystals of **1** was monitored by completely dissolving the crystals in acetone and measuring by gas chromatography (Figs. 3a

The crystals of **1** form with longer containing 14 carbon selectivity independent immersing time (Fig. S17).



and S17). activated tended to complexes *n*-alkanes more than atoms. The was of the time (Fig.

Fig. S17 Gas chromatograms of host-guest complex crystals of **1** after immersing in equal volume of *n*-alkane mixtures at 25 °C for (a) 10, (b) 20, (c) 60, (d) 120 and (e) 180 s.

3.4 Selective Uptake *n*-Alkanes from 1:1 Mixture of *n*-Alkanes by Activated Crystals of **1**

Activated crystals of **1** (20 mg) was immersed in a sealed 5 mL vial containing bulk *n*-alkanes consisting of equal volume of two different *n*-alkanes at 25 °C for 24 h. To remove un-complexed *n*-alkanes, the crystals were washed with cyclohexane. Composition of *n*-alkane guests up-taken by activated crystals of **1** was monitored by completely dissolving the crystals in acetone and measuring by gas chromatography (**Fig. 3b**). The feed ratios of the two different *n*-alkanes did not effect on the sorting (**Fig. S18**).

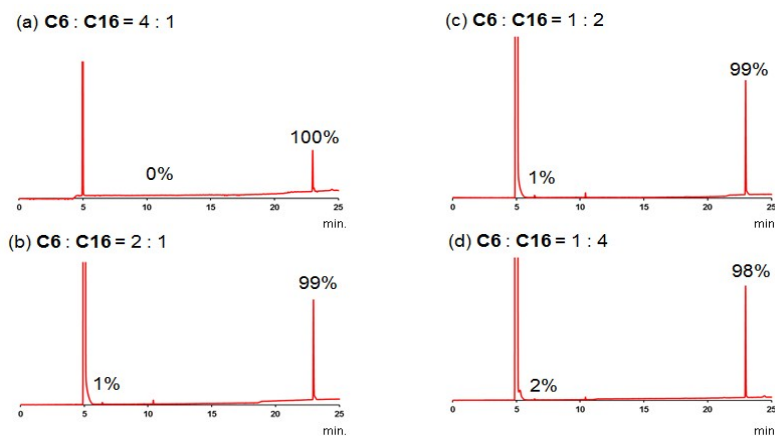


Fig. S18 Gas chromatograms of crystals of **1** after immersing in a liquid containing **C6** and **C16** in (a) 4:1, (b) 2:1, (c) 1:2 and (d) 1:4 ratios. The feed ratio did not effect on the sorting.

4. Computational Details

To identify how the origin of the selectivity is achieved, we calculated the binding energies for the complexes using molecular mechanics (MM) simulations. Three models of complexes were examined. Model 1 is the simplest model containing one *n*-alkane molecule and one pillar[5]arene molecule. Two other more advanced models were also used; model 2 is a simplified model for a herringbone structure, while model 3 is a model of a one-dimensional channel structure. In **Fig. 3c**, we can see that in model 1, the binding energy increases gradually with increasing chain length of *n*-alkane. This trend can be understood in terms of larger van der Waals attraction that longer *n*-alkanes can gain upon complexation. In comparison, the binding energy values behaved somewhat differently in model 2. In this model, the binding energy decreased at some point after **C7**, and it later increased again, but not as significantly as it did in model 1. Of note, there is a decrease in binding energy in going from **C7** to **C8** in model 2. This

decrease should be due to slight protrusion of **C8** of the pillar[5]arene cavity, and the protrusion results in somewhat less efficient binding between neighboring pillar[5]arenes in the herringbone structure. In fact, model 3 gives much larger binding energies than model 2, and this trend is attributed to the fact that the protruding atoms are covered effectively by another pillar[5]arene molecule in the one-dimensional channel structure. As with model 1, model 3 exhibited a monotonic increase in binding energy, and the increase was more rapid in model 3. The supporting role of another pillar[5]arene molecule in stabilizing the protruding part of longer *n*-alkanes is evident from the difference in binding energy between models 1 and 3 (“model 1 – model 3” in **Fig. 3c**), because this value increases monotonically with increasing chain length. The calculated binding strength for **C7** was slightly larger in model 3 than in model 2, and this result is not perfectly consistent with the experimental observation of a herringbone structure in the complex of **C7**. Nevertheless, in view of the simplicity of the models employed and the limited accuracy of MM calculations, one can argue that the binding energy values summarized in **Fig. 3c** well capture the general trend in the preference for the one-dimensional channel structure in longer *n*-alkanes, which in turn allows cooperative binding. In addition, the tendency of longer *n*-alkanes, especially **C13–C16**, to bind more strongly to pillar[5]arene is also well reproduced.

5. References

- S1) T. Ogoshi, K. Kitajima, T. Aoki, S. Fujinami, T. Yamagishi and Y. Nakamoto, *J. Org. Chem.*, 2010, **75**, 3268.
- S2) BIOVIA Materials Studio 8.0, BIOVIA, San Diego, CA, 2015.
- S3) H. Sun, *J. Phys. Chem. B*, 1998, **102**, 7338
- S4) H. Sun, Z. Jin, C. Yang, R. L. C. Akkewemans, S. T. Robertson, N. A. Spenley, S. Miller and S. M. Todd, *J. Mol. Model.*, 2016, **22**, 47.